Electronic Supplemental Information for

Water-Resistant $AgBiS_2$ Colloidal Nanocrystal Solids for Eco-friendly Thin Film Photovoltaics†

Jae Taek Oh,[ab] Sung Yong Bae,[ab] Su Ryong Ha,[a] Hongjoo Cho,[a] Sung Jun Lim,[c] Danil W. Boukhvalov,[d] Younghoon Kim*[b] and Hyosung Choi*[a]

[a] Department of Chemistry and Research Institute for Natural Sciences, Hanyang University, 222 Wangsimni-ro, Seongdong-gu, Seoul 04763, Korea

[b] Convergence Research Center for Solar Energy, Daegu Gyeongbuk Institute of Science & Technology (DGIST), 333 Techno Jungang-Daero, Hyeonpung, Daegu 42988, Korea

[c] Intelligent Devices and Systems Research Group, Daegu Gyeongbuk Institute of Science & Technology (DGIST), 333 Techno Jungang-Daero, Hyeonpung, Daegu 42988, Korea

[d] Theoretical Physics and Applied Mathematics Department, Ural Federal University, Mira Street 19, 620002 Yekaterinburg, Russia

* Corresponding Authors

E-mail: younghoon.kim@dgist.ac.kr and hschoi202@hanyang.ac.kr

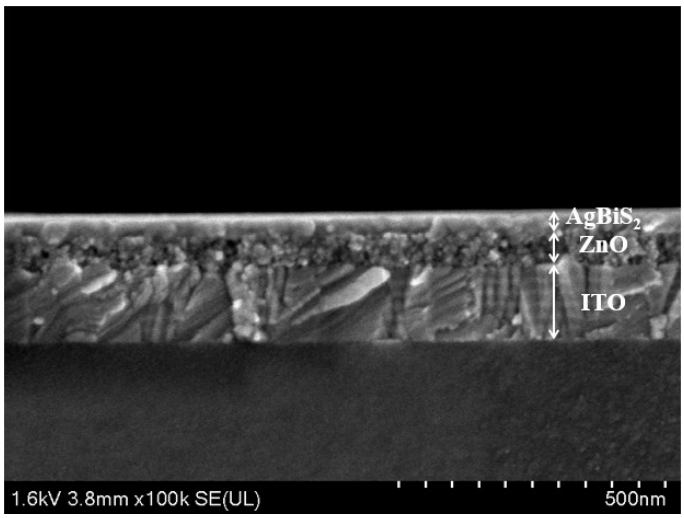

Fig. S1 Cross-sectional SEM image of $AgBiS_2$ nanocrystal thin film onto a ZnO-coated ITO substrate after solid-state ligand exchange process.

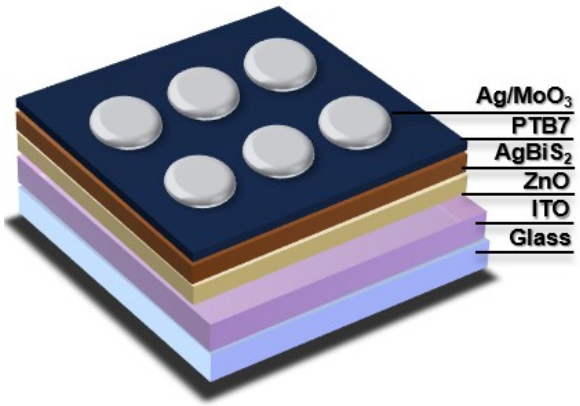

Fig. S2 Schematic illustration of the $AgBiS_2$ nanocrystal solar cell.

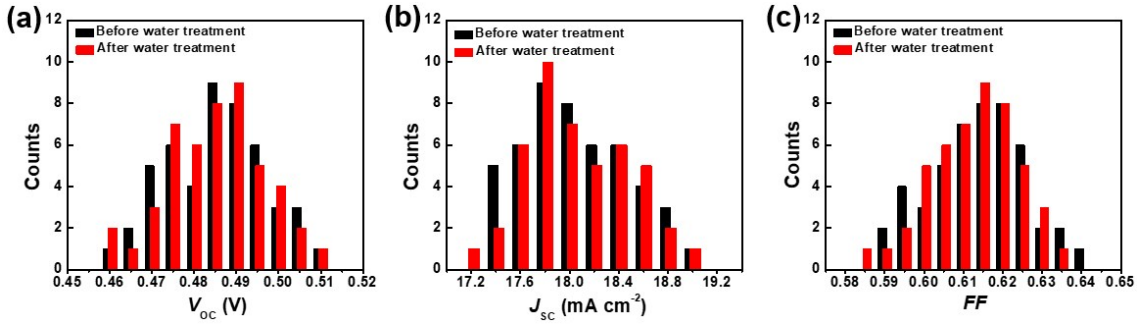

Fig. S3 Device histograms for $AgBiS_2$ solar cells before and after the water treatment: (a) V_{OC}, (b) J_{SC}, and (c) *FF*, respectively.

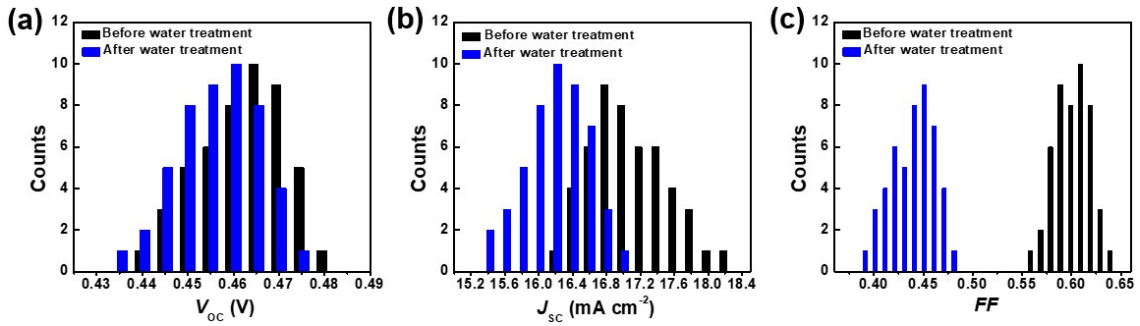

Fig. S4 Device histograms for PbS CQD solar cells before and after the water treatment: (a) V_{OC}, (b) J_{SC}, and (c) *FF*, respectively.

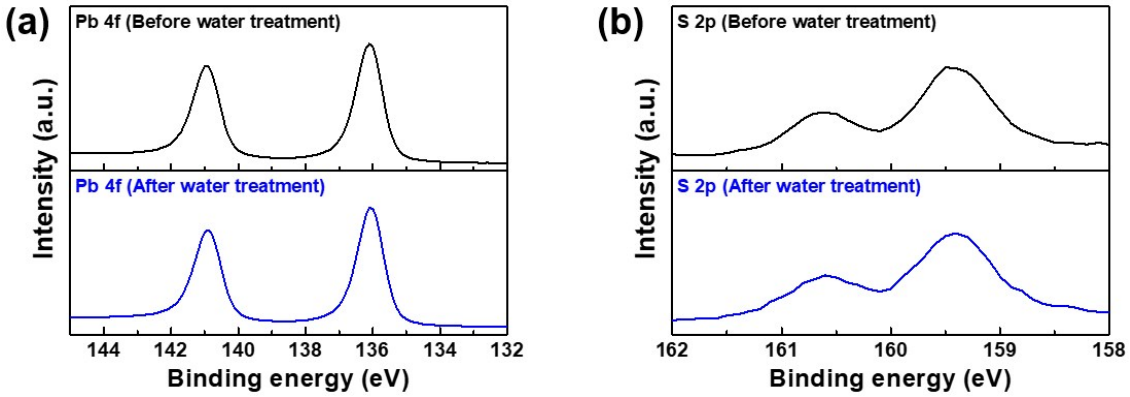

Fig. S5 (a) Pb 4f, (b) S 2p XPS spectra of the PbS CQD thin films before and after the water treatment.

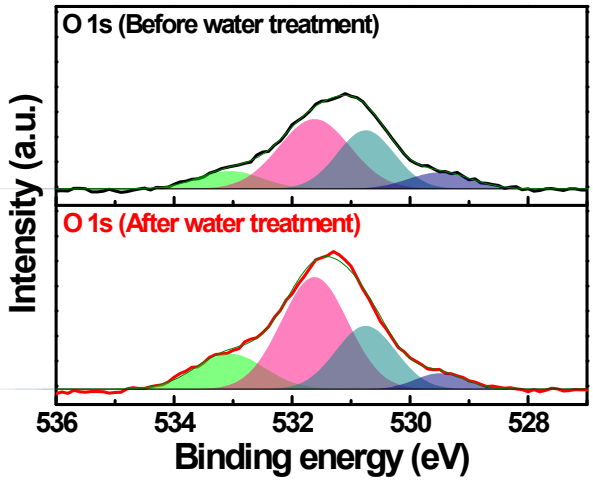

Fig. S6 O 1s XPS spectra of $AgBiS_2$ nanocrystal thin films before and after water treatments.

Table S1. Relative amounts of each element found by XPS of PbS CQD thin films before and after water treatment.

Sample	Pb	S(2p)	O	I
Before water treatment	1.00	0.67	0.70	0.37
After water treatment	1.00	0.66	0.99	0.25

Quantities normalized to Pb.

Table S2. Relative amounts of each element found by XPS of $AgBiS_2$ nanocrystal thin films before and after water treatment.

Sample	Ag	Bi	S(2p)	O	I
Before water treatment	2.87	1.00	0.86	1.57	1.40
After water treatment	2.78	1.00	0.87	2.23	1.35

Quantities normalized to Bi.

The atomic structure and energetics have been studied by DFT using the QUANTUM-ESPRESSO code[S1] and GGA–PBE approximation[S2], which are feasible for the description of the solids. During the optimization, the ion cores were described by norm-conserving pseudo-potentials[S3]. We used energy cutoffs of 25 Ry and 400 Ry for the plane-wave expansion of the wave functions and the charge density, respectively. Optimization of the force and total energy was performed with an accuracy of 0.04 eV/Å and 1 meV, respectively. For the modeling of $AgBiS_2$ surfaces, we first made supercell of 108 atoms and further increase lattice parameters along each crystallographic direction. Thus, we create 3 slabs corresponding with (001), (100) and (010) surfaces (**Fig. S7**). For (100), (001) and (010) surfaces we used the 2×4×4, 4×4×2 and 4×2×4 Monkhorst-Pack *k*-point grid for the Brillouin sampling respectively[S4]. For the modeling of PbS(001) surface we used the slab of 64 atoms (**Fig. 5b** in the main text). Modeling of (111) surface of PbS required larger number of atoms (71, see **Fig. S8**). For both surfaces we used 4×4×2 Monkhorst-Pack *k*-point grid. The difference in the number of atoms in supercell caused difference in the number of the atoms in unit cell between $AgBiS_2$ and PbS. The difference in the number of atoms in supercells used for the modeling of PbS is originated from the larger number of atoms in each layer.

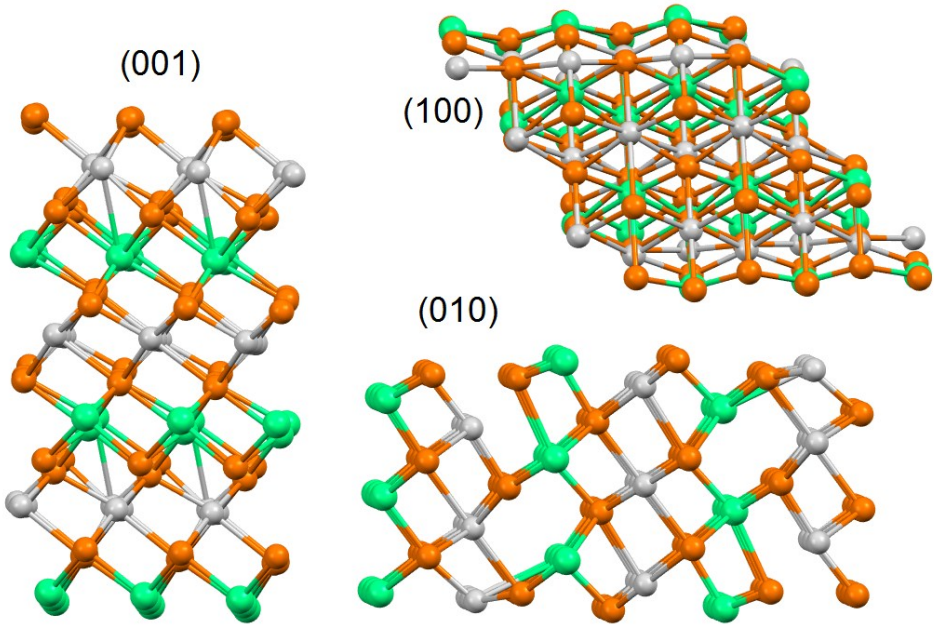

Fig. S7. Optimized atomic structure of the slab used for the modeling of (001), (100) and (010) surface of $AgBiS_2$. Bismuth, silver and sulfur atoms are shown in green, light grey and brown

colors, respectively. Note that the break between silver and sulfur atoms in subsurface layer is artefact of the software used for visualization.

Owing to the differences in the ionic radii and oxidation states of silver and bismuth, the crystal structure of $AgBiS_2$ is similar to that of cubic rock-salt (Schapbachite) only at temperatures above 200 °C and changes to a rhombohedral structure (Matildite) at room temperature[S5]. In this rhombohedral structure, the (111) crystallographic planes of the cubic rock-salt structure transform into three additional planes: (100), (010), and (001). Therefore, in our model, we assumed that $AgBiS_2$ has a rhombohedral structure with (100), (010) and (001) surfaces. It is well-known that PbS CQDs largely have (001) and (111) surfaces. Therefore, we considered two types of PbS(001) and (111) surfaces with a rock-slat crystal structure (**Fig. 5b and Fig. S8**).

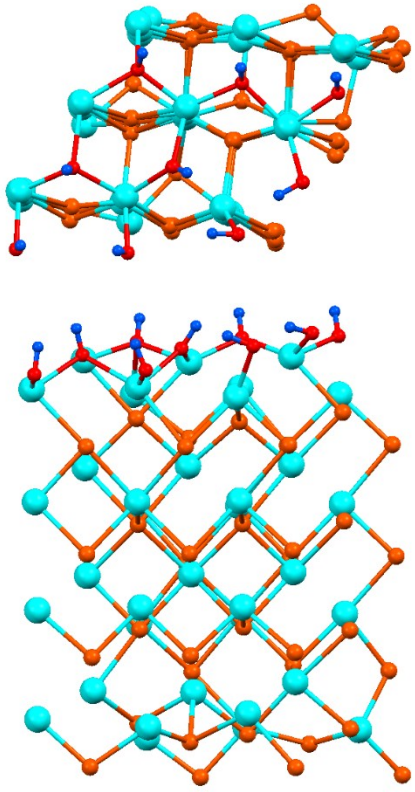

Fig. S8 Top and side view of the optimized atomic structure of the PbS(111) surface passivated using hydroxyl groups on Pb-terminated side. (Cyan, orange, red, and blue colors indicate Pb, S, O, and H, respectively.)

As the first step in the calculations, we examined the effect on the passivation of the various $AgBiS_2$ surfaces: Bi- or S-terminated (001) surface, Bi- and S-terminated (100) surface (note that Ag atoms are located below approximately 0.2 Å, compared to Bi and S atoms, **Fig. S7**) and Ag-terminated (010) surface, which Ag atoms are available for interactions. We calculated the binding energies of iodine on all the $AgBiS_2$ surfaces using the expression given below:

$$E_{bind} = E_{pure\ surface} + E(I_2)/2 - E_{passivated\ surface} \quad (1)$$

The total energy of iodine is calculated for the gaseous phase. For this we put the single I_2 molecule in the center of the unit cell $10\times10\times10$ $Å^3$ and perform optimization of atomic positions.

For the recognition of the active sites on the surface we checked the difference in the charge of the atoms on the surface. Because the calculated charges of the atoms of the same type on surface and in bulk were different, we considered that these surface sites are active. For all types of the surfaces we discuss only the case of adsorption on all active sites. We found that the iodine binding energies at the $AgBiS_2$(100), (010), and (001) surfaces are higher than those at the PbS(001) and (111) surfaces, indicating that iodine binds strongly to the $AgBiS_2$ surfaces. The calculation results are given in **Table 3**.

As the second step during modelling, we evaluated the relative stability of iodine in water environments and calculated the total energy (i.e., energy cost) required for the substitution of iodine by hydroxyl groups as shown below:

substrate-I + H_2O → substrate-OH + HI

using the expression:

$$E(I\leftrightarrow OH) = E(\text{substrate-OH}) - E(\text{substrate-I}) + E(H_2O) - E(HI), \quad (2)$$

where E(I↔OH) is the total energy required for the substitution of iodine by hydroxyl groups. E(substrate-I), E(substrate-I), E(H_2O), and E(HI) are the energies of the iodine- and OH-passivated surfaces and those of H_2O and HI in the gas phase, respectively. The total energies of the $AgBiS_2$ (100), (010), and (001) surfaces were calculated to be 0.92, 1.59, and 1.26 eV,

respectively, while those of the PbS(100) and (111) surfaces were determined to be 1.71 and 1.48 eV, respectively (**Table 3**). Hence, the energy costs for the PbS surfaces are as high as those for the $AgBiS_2$ surfaces; this was in contrast to the experimental results, which indicated that the iodine is removal and that the surfaces of the PbS CQDs undergo hydroxylation after the water treatment (**Fig. 4c and Fig. S4**). These differences in the binding energies are related with the different magnitude of local distortions (see **Table S3**). The larger deviation of the atomic positions from stoichiometric is corresponding with larger magnitudes of iodine formation energies. For example, the largest deviation and the largest iodine binding energy are corresponding with (001) surface of $AgBiS_2$. Unfavourability of the substitution of iodine to hydroxyl group on the surfaces of $AgBiS_2$ caused by increasing of the local distortions after the substitution.

Instead, we considered the oxygen-containing PbS surfaces, which are formed by the substitution of sulfur with oxygen, because the TMAI-exchanged PbS solids showed O 1s XPS peaks related to oxygen-containing species (i.e., Pb−O bonds) both before and after the water treatment (**Fig. 4d**). Thus, we calculated the formation energies of PbO by the substitution of sulfur with oxygen using the following expression:

$$E = [E(PbO) - E(PbS) + nE(O_2)/2 - nE(S_2)/2]/n, \quad (3)$$

where E(PbS) and E(PbO) are the total energies of the surface before and after the substitution of sulfur by oxygen, respectively, $E(O_2)$ and $E(S_2)$ are the total energies of oxygen and sulfur in the gas phase, respectively; and n is the number of substituted atoms. The calculation results showed that PbO formation on the iodine-passivated PbS(001) and (111) surfaces is energetically favorable because the degree of distortion in an out-of-plane direction owing to the substitution of the sulfur atoms by the oxygen atoms is lower (see **Table S3**), since oxygen atoms are smaller (ionic radii of sulfur and oxygen are 1.84 and 1.38 Å, respectively). We also determined the formation energy of $AgBiO_2$ on the Ag-terminated $AgBiS_2$(010) surface using Eq. (3). The calculation results suggested that this process is also energetically favorable but not to the same degree as the formation of PbS. Further, this result can be attributed to the initial distortion of the $AgBiS_2$ surface with the matildite crystal structure (**Table S4**).

Table S3. The mean deviation (in %) of interatomic distances in the used slabs for the different bare and passivated surfaces of $AgBiS_2$, PbS and PbS with surface PbO layer (denoted in the table as PbO).

Material	Surface	bare	-I	-OH
$AgBiS_2$	001	2.9	2.9	3.1
	100	2.2	2.4	2.5
	010	2.2	1.9	2.5
PbS	001	2.4	3.2	3.3
	111	2.5	3.3	3.4
PbO	001	1.9	2.4	2.0
	111	2.2	2.5	2.3

Table S4. Formation energies of PbO and $AgBiO_2$ on PbS(001) and $AgBiS_2$(010) surfaces by the substitution of sulfur with oxygen (value within parentheses is formation energy of PbO on PbS(111) surface).

	PbS to PbO	**$AgBiS_2$ to $AgBiO_2$**
Formation energy (eV)	−0.20 (−0.46)	−0.06

We calculated the energy cost for the substitution of iodine with hydroxyl groups on the PbO(001), (111) and $AgBiO_2$(010) surfaces and found that the energy cost in the case of the PbO(001) and (111) surfaces is significantly lower, suggesting that the substituion of iodine with hydroxyl groups on PbO is energetically much more favorable than in the case of $AgBiO_2$ (**Table 4**). The calculation results corresponded well with the XPS results, which also suggested the removal of iodine and the surface hydroxylation of PbS after the water treatment.

References:

[S1] P. Giannozzi, S. Baroni, N. Bonini, M. Calandra, R. Car, C. Cavazzoni, D. Ceresoli, G. L. Chiarotti, M. Cococcioni, I. Dabo, A. Dal Corso, S. de Gironcoli, S. Fabris, G. Fratesi, R. Gebauer, U. Gerstmann, C. Gougoussis, A. Kokalj, M. Lazzeri, L. Martin-Samos, N. Marzari, F. Mauri, R. Mazzarello, S. Paolini, A. Pasquarello, L. Paulatto, C. Sbraccia, S. Scandolo, G. Sclauzero, A. P. Seitsonen, A. Smogunov, P. Umari and R. M. Wentzcovitch, *J. Phys. Condens. Matter*, 2009, **21**, 395502.

[S2] J. P. Perdew, K. Burke, M. Ernzerhof, *Phys. Rev. Lett.* 1996, **77**, 3865-3868.
[S3] O. N. Troullier, J. L. Martins, *Phys. Rev. B* 1991, 43, 1993.
[S4] H. J. Monkhorst and J. D. Pack, *Phys. Rev. B*, 1976, **13**, 5188-5192.
[S5] S. Geller, J. H. Wernick, *Acta Crystallogr.*, 1997, **12**, 46−54.